# Supplementary Information

## Single-molecule mechanical study of an autonomous artificial translational molecular motor beyond bridge-burning design

Xinpeng Hu, Xiaodan Zhao, Iong Ying Loh, Jie Yan, Zhisong Wang*

**More information on materials and methods**

(1)Measurement of bead displacement (Figure S1)
(2)Fabrication of 800bp DNA tether
(3)Channel preparation for motor-track assembly and operation
(4)Optimization of in-situ assembly
(5)DNA sequences (Figure S2)

**Extra data (Figure S3 – S10)**

Figure S3. Control trajectory for 1.5pN without fuel, and force-induced leg dissociation.
Figure S4. Control trajectory for 0.6 pN without fuel.
Figure S5. Typical trajectory of the motor at 1.5 pN and 1 μM fuel.
Figure S6. A typical trajectory recorded under a nearly stalling force of 2 pN at 0.5 μM fuel.
Figure S7. A typical trajectory at an above-stall force of 3 pN and 0.5 μM fuel.
Figure S8. Stable-dwell segments from the trajectory in Figure 2A.
Figure S9. Stepping analysis by a standard step finder algorithm.
Figure S10. The motor's load-dependent directionality and stall force estimated from biases associated with two equal-sized ~ 8nm half steps.

**More information on materials and methods**

**(1)Measurement of bead displacement**

In the magnetic tweezers, a key quantity to measure is the change of the bead's vertical displacement above the coverslip surface (i.e., *z* axis in Figure 2, 3, etc.). The bead height is obtained through image analysis of the diffraction patterns recorded by a CCD (charge-coupled device) camera. The methods are elaborated in an early reference[1], and also in a recent publication[2] from coauthors of this paper (Xiaodan Zhao and Jie Yan). The diffraction of the bead has a typical ring pattern. The change of the ring pattern is sensitive to the bead's distance from the focal plane of the objective in the microscope. Figure S1 below shows representative diffraction patterns of the bead used in this study at different bead-focal plane distance. In this manner, an initial library of bead images at different focal planes is recorded by changing the objective focal plane using a high-precision piezo scanning stage. During experiments, the bead height is determined by maximum cross-correlation between the image and the library built from the same bead.

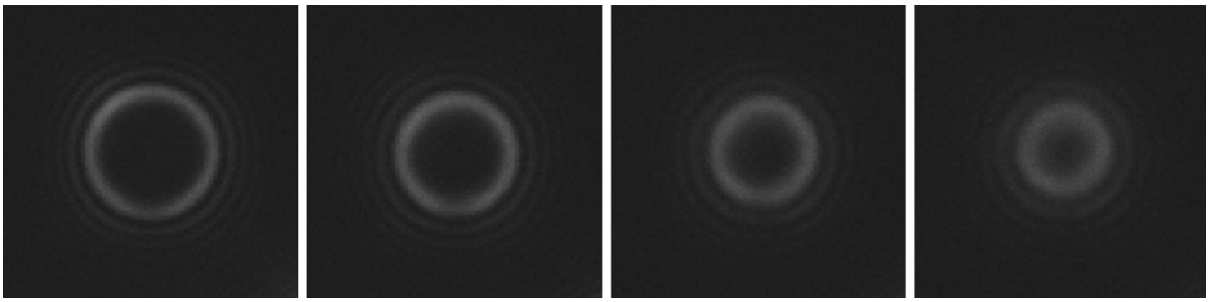

Figure S1. Representative diffraction patterns of the bead away from the objective's focal plane with 0.5 mm increasement step from left to right

**(2)Fabrication of 800bp DNA tether**

For the DNA tether, we choose from lambda DNA a 765bp sequence that contains a recognition site for restriction enzyme SMAI (CCC^GGG, ^ for cutting site) for the designed bead shift but does not have the recognition site for the nicking enzyme required for the motor's operation. The 765bp segment is amplified by PCR (polymerase chain reaction), and further modified into a 800bp duplex tether with one strand labeled with biotin at 5' end and thiol at 3' end. The procedure for the tether fabrication is schematically illustrated below, with experimental steps explained afterwards.

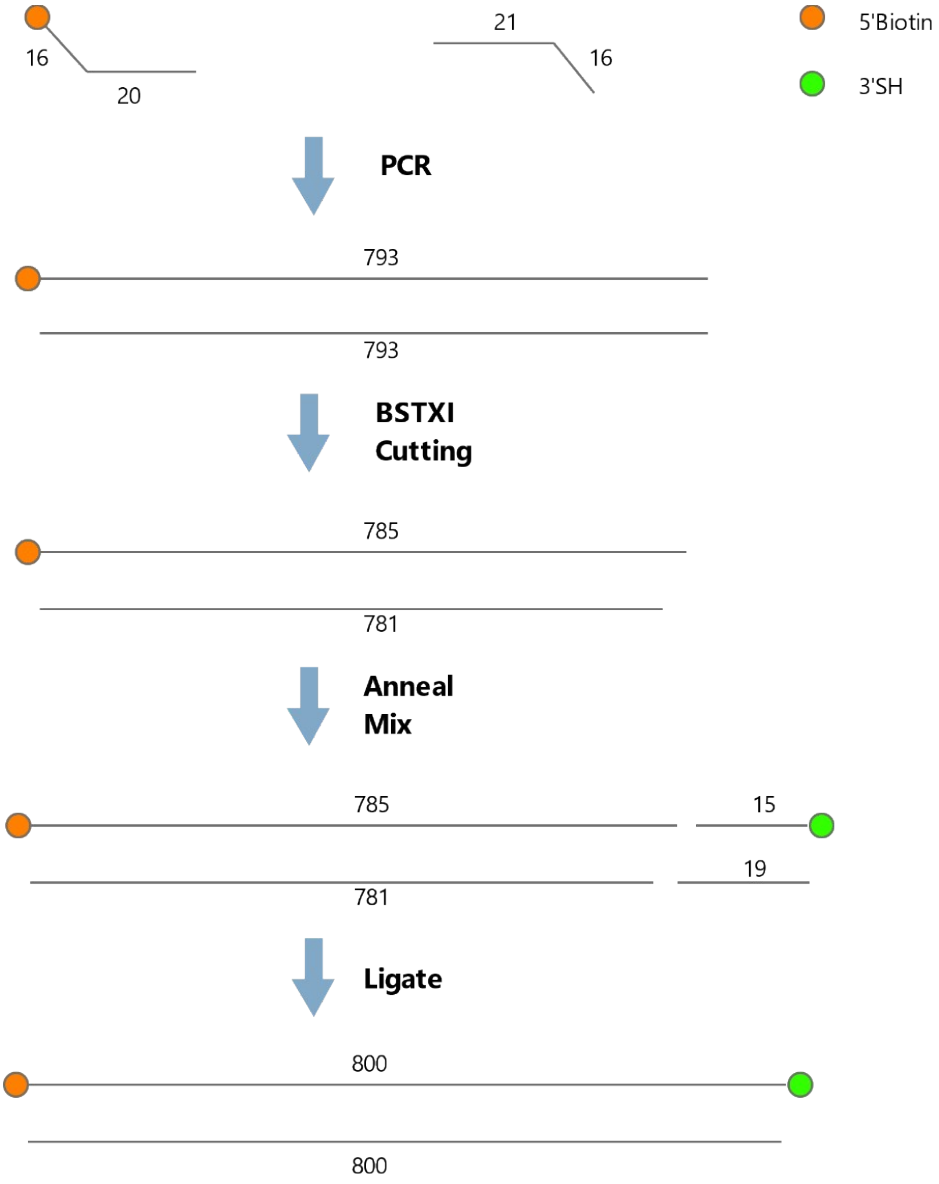


**Schematic illustration of experimental steps for tether fabrication.**

First, PCR is done using two primers that have extra sequences (underlined segments in primer sequences shown below) to introduce either biotin or a cutting site for a restriction enzyme BSTXI for later thiol labelling.
PrimerTop: 5' - /5biosg/TTAAGCACACTCAAGG ACGATGGAACAGGTTAACGC -3'
PrimerBtm: 5' - TTAACCATTCGG^ATGG TAATGTAGATGGTCATCTTTT -3'

PCR is carried out on BioRad Thermal Cycler C1000 Touch. PCR mix is prepared as follows: 151 µl DI water; 4µl dNTP solution mix (NEB); 1µl Lambda DNA (NEB); 1µl PrimerTop (100uM, IDT); 1µl PrimerBtm (100uM, IDT); 40µl Q5 Reaction Buffer (5x, NEB); 2µl Q5 Polymerase (NEB). For the thermal cycles, an initial denaturation (98°C, 30 seconds) is followed by 25–35 cycles (98°C, 10 seconds plus 72°C, 44 seconds per cycle), and then a final extension (72°C, 2 minutes before 4°C hold). After PCR, the sample is purified with Invitrogen's Purelink PCR Purification Kit. The purified product (~ 793bp) is quantified with ThermoFisher Nanodrop One (~ 1uM).

Second, the purified PCR product is digested at one end by BSTXI cutting, with the following protocol: 50µl PCR product; 30 µl DI water; 15µl NEB 3.1 buffer; 5µl BSTXI (NEB Stock). After a long incubation (37°C, ~12 hours), the sample goes through the same purification process as before. The yield for the purified product (~ 781bp) is around 70%.

Third, the tether is formed by ligation of a short thiol duplex to the digested PCR product. The thiol duplex is prepared from two strands (sequences shown below) by annealing (5 minutes of 98°C followed by 40 minutes of gradual cooling to room temperature). The final duplex is 50µM in concentration, with a salty solution of 50mM of potassium ions.
TempThiolA (15): 5'- /5Phos/GCTTGAAGAGCTAGA/3ThioMC3-D/ -3'
TempThiolB (19): 5'- TCTAGCTCTTCAAGCATCC -3'

The ligation is achieved as the following mix: 46µl of digested PCR product; 2µl of thiol duplex (50 µM); 6µl of T4 ligation buffer (10x, NEB); 6µl of T4 ligation enzyme (NEB). After 1 hour incubation at room temperature, the sample is further mixed with12 µl of SDS-dye and run in 1% agarose gel. The band corresponding to ~ 800bp is extracted and purified using Invitrogen Gel Purification Kit. The final product is usually around 20ng/µl for concentration.

The three experimental steps of PCR, digestion and ligation finally produce a 800bp double-stranded tether with one strand as /5biosg/-800 nucleotides-/3thiol-mc/ (detailed sequence given in a later section).

**(3)Channel preparation for motor-track assembly and operation**
The glass channel for the motor-track assembly and later operation is made of a cover glass (0.1mm thick) and a glass slide (0.2mm thick), glued together by hydrophobic striped parafilm (for blocking liquid leaks). Before the channel integration, the cover glass and slide are carefully cleaned (critical for single-molecule experiments). The glass slide goes through more thorough cleaning as well as a coating ((3-Aminopropyl) triethoxysilane, APTES) to functionalize its surface for the purpose of tether immobilization.

The cover glass is sonicated for 5 minutes in 5% detergent, and then rinsed by DI (deionized) water and dried in the oven. It is first sonication in detergent, DI water, acetone and methanol subsequently (5 minutes for each solvent) before drying up in oven. Next, it is plasma cleaned under high intensity for 15 minutes. Afterwards, a 50ml 1% APTES solution (solvent: methanol) is prepared with which the slip is incubated for 45 minutes. The slip is further cleaned with methanol followed by 5 minutes sonication in methanol and ethanol respectively before drying again in the oven.

Our tweezers experiments each are started with channel integrated from the cleaned components by heated parafilm strips. In the meanwhile, the DNA tether is prepared by diluting the previously purified tether sample (5:50) and adding dithiothreitol to reduce oxidization of thiolated DNA. The solution containing reference beads (1:300, 1xPBS) is first added to the channel. After 5 minutes incubation, the channel is washed by 1mL of 1xPBS (pH=7.4). For surface functionalization, sulfo-SMCC is dissolved initially using DI water and then mixed with 2xPBS. The resulting solution is flushed into the channel and kept for 5 minutes. After the channel is washed again with 1mL of 1xPBS, the tether sample is incubated for 30 minutes inside the channel for tether binding. Then the channel is washed with 2% BSA (with 0.1% 2-mercaptoethanol in 1 x PBS), sealed in a petri dish, and kept in 4°C overnight before the motor-track assembly and operation experiment.

**(4)Optimization of in-situ assembly**
Different procedures for the in-situ motor-track assembly are attempted and finally optimized, as elaborated below.

Procedure 1: Force-assisted room-temperature assembly of the whole track (excluding Site1a and Site2a strands) plus pre-fabricated motor complex. The room-temperature hybridization of track strands to the 800nt-long template is done in the channel under a stretching force of 20 pN (typical data shown in Figure 1F and Figure 1G). For the motor complex, two hot-annealed products are separately prepared outside the channel: Site1a and MotorLB for one; Site2a, MotorLA, and Handler for the other (see Figure S2 for strand labels). The two hot-annealed products are mixed for long incubation before being introduced into the channel. The motor complex is presumably guided by Site1a and Site2a strands to hybridize with the template-track at the first and second binding sites. But this motor-track assembly procedure fails as the bead quickly disappears (< 1 minute) after SMAI is introduced. The outcome is not improved even with agarose gel purification of the motor-handler-site1a-site2a complex before its adding to the channel. A possible reason is that this complex might also hybridize with the template at other binding sites and there are 10 sites in total. To avoid this problem, the two hot-annealed products are not mixed but directly introduced into the channel in a right order: first the MotorLB+Site1

product and then the MotorLA+Site2a+Handler (5 minutes or longer incubation for each product for hybridization to the template-track in the channel). But still no improvement is obtained.

Procedure 2. Complete room-temperature hybridization of all strands inside the channel. For site-specific formation of the motor (at 1$^{st}$ and 2$^{nd}$ sites), the strands are flowed into the channel with the bead-controlled 800nt-long template in an orderly manner as shown in Figure 1C. The sequential addition splits the whole process of motor-track assembly into individual hybridization steps with controlled strand availability to avoid unwanted hybridization events between the many strands (26 in total). During a hybridization step, a strand designed to bridge two other strands might have two copies of the first strand separately joining the two latter strands, thus jeopardizing the intended hybridization. One example is the longer half motor (MotorLA) that might have one copy hybridizing with the other half motor (MotorLB on site1a) and a second copy hybridizing with Site2a. Another example is handler strand connecting the motor and the template. The problem is mitigated by decreasing concentration for the two bridging strands as the separate hybridizations require two copies for either strand (only one copy needed for the intended hybridization). The new assembly procedure is successful as indicated by continued bead presence after SMAI cutting.

The assembly procedure is further optimized by parameter/condition adjustments as follows.

1. Force adjustment, e.g., lowering the pulling force on the template from 20 pN to ~ 4 pN for the hybridization steps involving bridging strands (e.g., long half motor and handler). This drastically improves success of the whole assembly process, likely because the single-stranded segment between the two hybridization partners for a bridging strand adopts a length suitable for the intended bridging hybridization (similar lengths are indeed found for single-stranded and double-stranded DNAs under ~ 4 pN in the present tweezers experiments).
2. Strand concentration (lower for bridging strands; ~ 300 nM is ok).
3. Higher salt concentration (50mM $K^+$ and 10mM $Mg^{2+}$ are enough).
4. Incubation time for individual hybridization steps (5 minutes ok for template-hybridizing strands and 15–20 minutes ok for other strands).

**(5)DNA sequences**

The sequences for all oligonucleotides used in this study are given in Figure S2, followed by the sequence for the 800nt-long template.

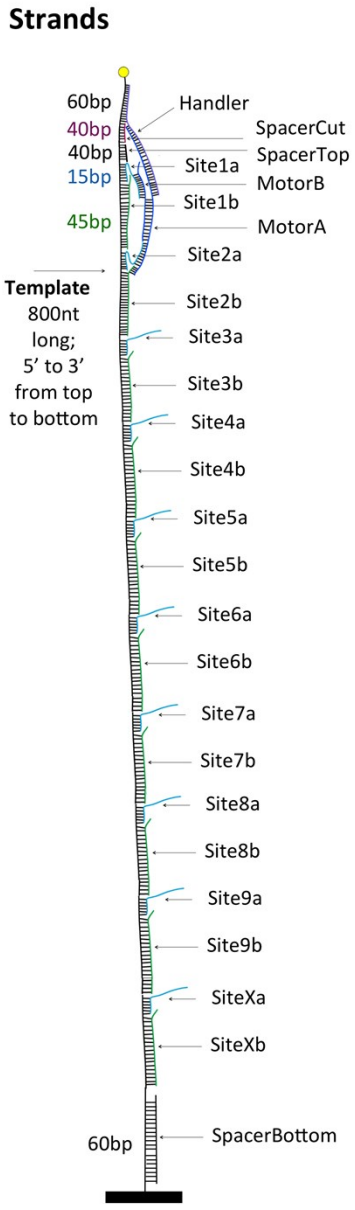


## Sequences

(all from 5' to 3')

**Handler:** AGACGACTAGCGGGACCTATTTTGTACCCTACTGCTGAATAACGGCGAGACAAGG
GTCTATAAAGCGGCGTGACTGTGTCCGGCTTCGTCATTTTCGAGAACCTAAGGACTTTTTTTTTTG
CCGACGGGCTACGCGCATTCCTGCGTTAACCTGTTCCATCGTCCTTGAGTGTGCTTAA

**SpacerCut:** TGCAACAAACTGCCC^GGGTGATGGCAGAAATGGTCGATTC
(^ for cutting site by SMAI)
**SpacerTop:** TTGGCAGTCCGGCGGTAACGGATGCTTCTTCCCGGCACCA

**MotorA:** GTCCTTAGGTTCTCGAAAATGACGAAGCCGGACACAGTCACGCCGCTTTATAGA
CCCTTGTCTCGCCGTTATTCAGCAGTAGGGTACAAAATAGGTCCCGCTAGTCGTCTTTTTTTTTTT
TACCATCTAGGTAGAGGCCGCTGAGGGCTGAGGTAAACT

**MotorB:** GGCCTCTACCTAGATGGTAAGCTGAGGGCTGAGGTAAACT

**Site1a:** CCAGCTCGCTGACGT TTTTTTTTTCTTCAGCCTTCAGC
**Site1b:** CCGGATACAGGCCTCGCTTCCGGCAATACTCGTAAACCATATCAA AGTTTA

**Site2a:** GATAAGACTCCGCAT TTTTTTTTTCTTCAGCCTTCAGC
**Site2b:** GATACAGGTTGGTAACCAGCCAGTAGTGCGCGTTTGATTTCCACG AGTTTA

**Site3a:** TGGCCCGCATGTTCT TTTTTTTTTCTTCAGCCTTCAGC
**Site3b:** GCTCATCTGCGGCCTTACGGCGTAATTCCGCATCAGTAAGCGCAT AGTTTA

**Site4a:** CAGTCATATGGACAA TTTTTTTTTCTTCAGCCTTCAGC
**Site4b:** GTTGTTTTACTGGTTCAGGGATCGCCTCACCACGGTTAATTCTCG AGTTTA

**Site5a:** CGCCCATGACAGGAA TTTTTTTTTCTTCAGCCTTCAGC
**Site5b:** TTTCTGCGATCTTCGCCAGAGCCTGTGCACGATTTAGAGGTCTAC AGTTTA

**Site6a:** CGAACTTAGCTTTGA TTTTTTTTTCTTCAGCCTTCAGC
**Site6b:** TGAATAATTGCCTCTTTGCCCGTCATACACTTGCTCCTTTCAGTC AGTTTA

**Site7a:** TGCGTCCCCAGGTAA TTTTTTTTTCTTCAGCCTTCAGC
**Site7b:** GTTGCGCCTGTTAGCGCGGCAACGTCCGGCGCACAGAAGCTATTA AGTTTA

**Site8a:** TTTATGCTGGTTACT TTTTTTTTTCTTCAGCCTTCAGC
**Site8b:** TCGATAACCAGAAGACCTGCCCGTGCCATTTTAGCCGCGGCCTGA AGTTTA

**Site9a:** CGCCAGACCTTACCT TTTTTTTTTCTTCAGCCTTCAGC
**Site9b:** TTTCCTTCCCGTTCTTCCCTGGTAGCAAACCGGTAATACACCGTT AGTTTA

**SiteXa:** AGGTTCGTGCTCATC TTTTTTTTTCTTCAGCCTTCAGC
**SiteXb:** AATACCCGTTTCATCGCGGCACTCTGGCGACACTCCTTAAAAACC AGTTTA

**SpacerBottom:**
TCTAGCTCTTCAAGCTCGGATGGTAATGTAGATGGTCATCTTTTAACTCCATATACCGCC

**Figure S2. DNA strands used in this study and their nucleotide sequences.** In addition, the motor's operation involves a fuel that is added to the solution and diffusively assesses the motor. The fuel is a short single-stranded DNA with sequence 5' - AGTTTACC^TCAGCCC^TCAGC - 3' (^ indicates cutting sites by nicking enzyme Nt.BbvCI, which recognizes the 7bp CCTCAGC sequence in the fuel-leg helix).

**Sequence for the 800nt-long template:**

/5biosg/TTAAGCACACTCAAGGACGATGGAACAGGTTAACGCAGGA
ATGCGCGTAGCCCGTCGGCAGAATCGACCATTTCTGCCATCACCCG
GGCAGTTTGTTGCATGGTGCCGGGAAGAAGCATCCGTTACCGCCGG
ACTGCCAAACGTCAGCGAGCTGGTTGATATGGTTTACGAGTATTGC
CGGAAGCGAGGCCTGTATCCGGATGCGGAGTCTTATCCGTGGAAAT
CAAACGCGCACTACTGGCTGGTTACCAACCTGTATCAGAACATGCG
GGCCAATGCGCTTACTGATGCGGAATTACGCCGTAAGGCCGCAGAT
GAGCTTGTCCATATGACTGCGAGAATTAACCGTGGTGAGGCGATCC
CTGAACCAGTAAAACAACTTCCTGTCATGGGCGGTAGACCTCTAAA
TCGTGCACAGGCTCTGGCGAAGATCGCAGAAATCAAAGCTAAGTT
CGGACTGAAAGGAGCAAGTGTATGACGGGCAAAGAGGCAATTATT
CATTACCTGGGGACGCATAATAGCTTCTGTGCGCCGGACGTTGCCG
CGCTAACAGGCGCAACAGTAACCAGCATAAATCAGGCCGCGGCTA
AAATGGCACGGGCAGGTCTTCTGGTTATCGAAGGTAAGGTCTGGCG
AACGGTGTATTACCGGTTTGCTACCAGGGAAGAACGGGAAGGAAA
GATGAGCACGAACCTGGTTTTTAAGGAGTGTCGCCAGAGTGCCGCG
ATGAAACGGGTATTGGCGGTATATGGAGTTAAAAGATGACCATCT
ACATTACCATCCGAGCTTGAAGAGCTAGA/3thiol-mc/

**Extra data (Figure S3 – S10)**

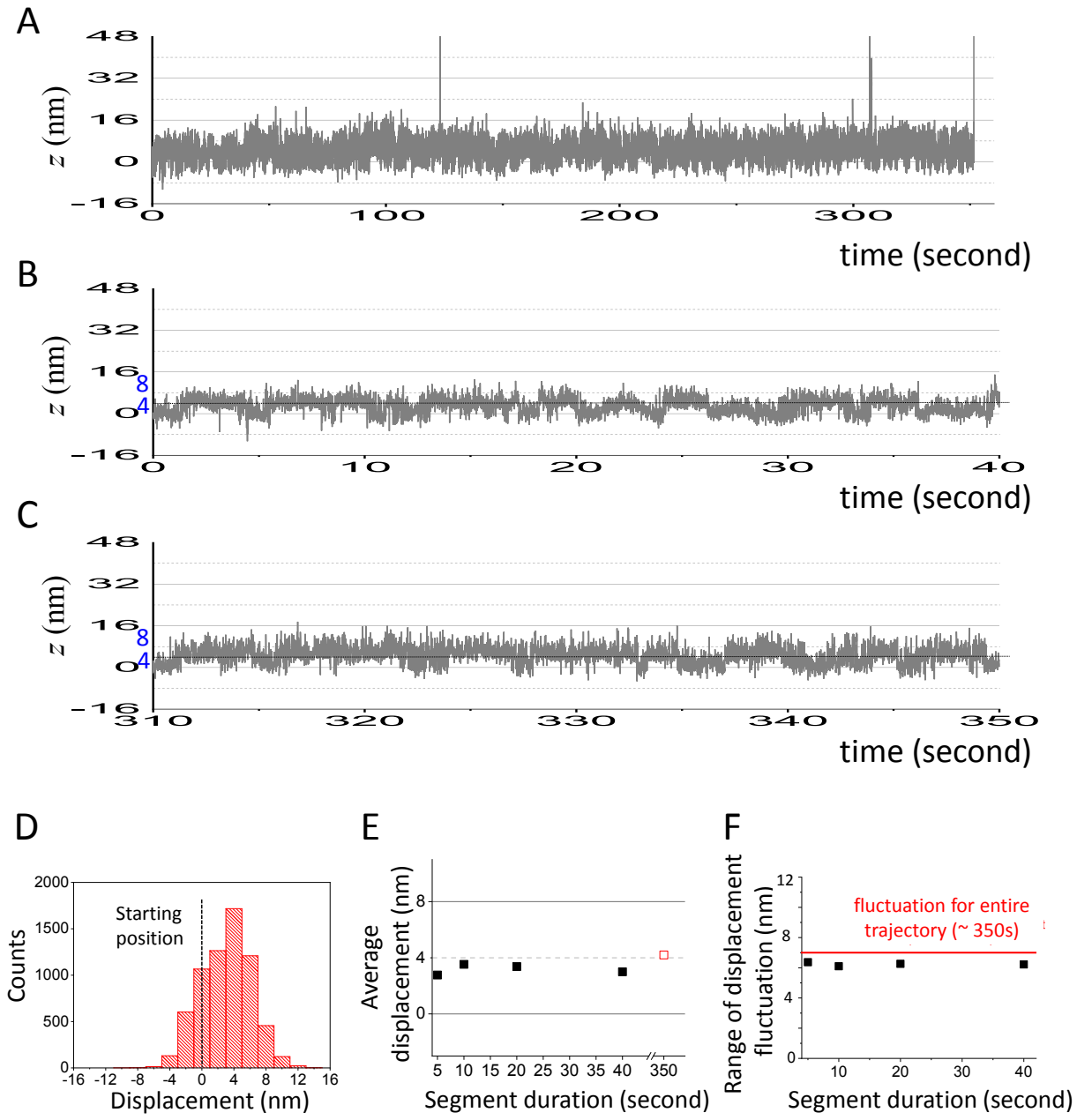


**Figure S3. Control trajectory for 1.5pN without fuel, and force-induced leg dissociation.** The trajectory is obtained from the same procedure as for operation trajectories (e.g., Figure 2A) except for zero fuel supply. The whole trajectory is presented in panel A, with details near the start and end shown in panels B, C. Panel D shows the distribution of displacement from the starting position extracted from the 40s long segment in panel B. Panel E presents the average displacement of the segment (different data points obtained from the segment by the same start but truncated at different duration as shown). Panel F gives the range of displacement fluctuation of the segment (i.e., two times the root-mean-square-displacement (RMSD) of each truncated

segment from its average position). The displacement and fluctuation are also obtained from the entire trajectory (red empty square in panel E and red line in panel F).

The data in panels D, E show that the most probable displacement and average displacement are both ~ + 4 nm for the starting 40s-long segment in panel B. In absence of fuel supply, this ~ 4nm backward displacement is caused by force-induced front leg dissociation from the initial two-legged bound state (state 1 in Figure 5), resulting in a single-legged state displaced ~ 4 nm backward from the motor's starting position (0 nm). The detailed segment in panel B indeed shows frequent ~ 4nm backward substeps and reverse forward ~ 4nm substeps resuming the motor's starting position. While the backward substeps correspond to the force-induced leg dissociation, the forward substeps correspond to reverse binding of the mobile leg to the site in front of the track-bound leg. Though the mobile leg is empty in this fuel-free control, the reverse forward substeps found here are equivalent of the transition from state 3 to state 5 in Figure 5. In other words, the average displacement of + 4 nm in panel E here is equivalent of -12 nm in Figure 4D. The fluctuations also match to some extent: the range of fluctuation for this fuel-free control experiment (~ 6 – 7 nm, see panel F) is understandably smaller but still close to that for the fuel-involved operation experiment (~ 8 – 12 nm, see Figure 4E). Compared to the starting segment, the segment in the end of the ~350s-long trajectory (panel C) also shows backward substeps and reverse forward substeps but with slightly larger displacement (probably due to elongated effects of the force).

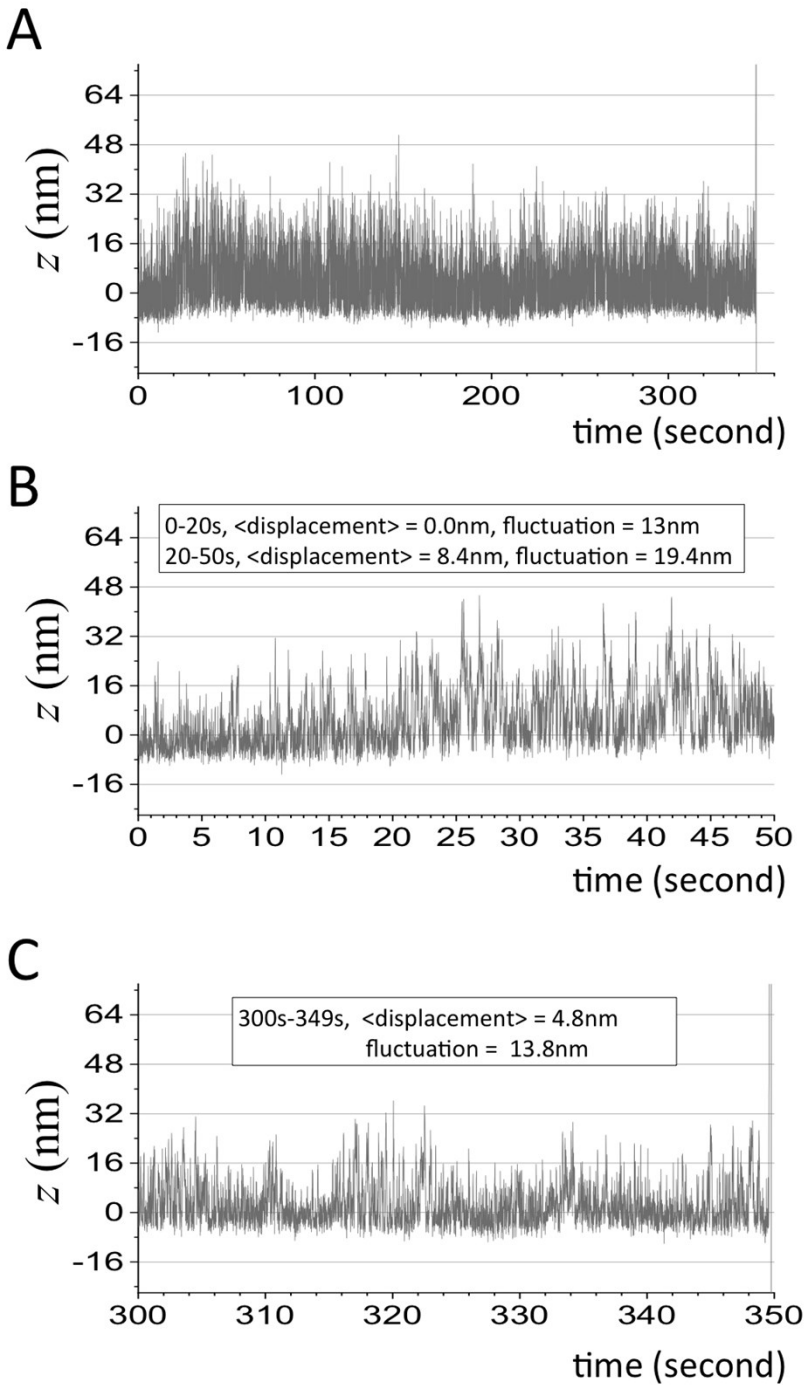


**Figure S4. Control trajectory for 0.6 pN without fuel.** The trajectory is obtained from the same procedure as for operation trajectories (e.g., Figure 3A) except for zero fuel supply. The whole trajectory is presented in panel A, with details near the start and end shown in panels B, C. The fluctuations at this low force are more than two times those of the control trajectory at 1.5 pN (see Figure S3, panel F), as shown for three representative segments in panels B, C (given in the panels are average displacement of the segments from the starting zero position and their range of displacement fluctuation, i.e., two times RMSD of each segment from its average position).

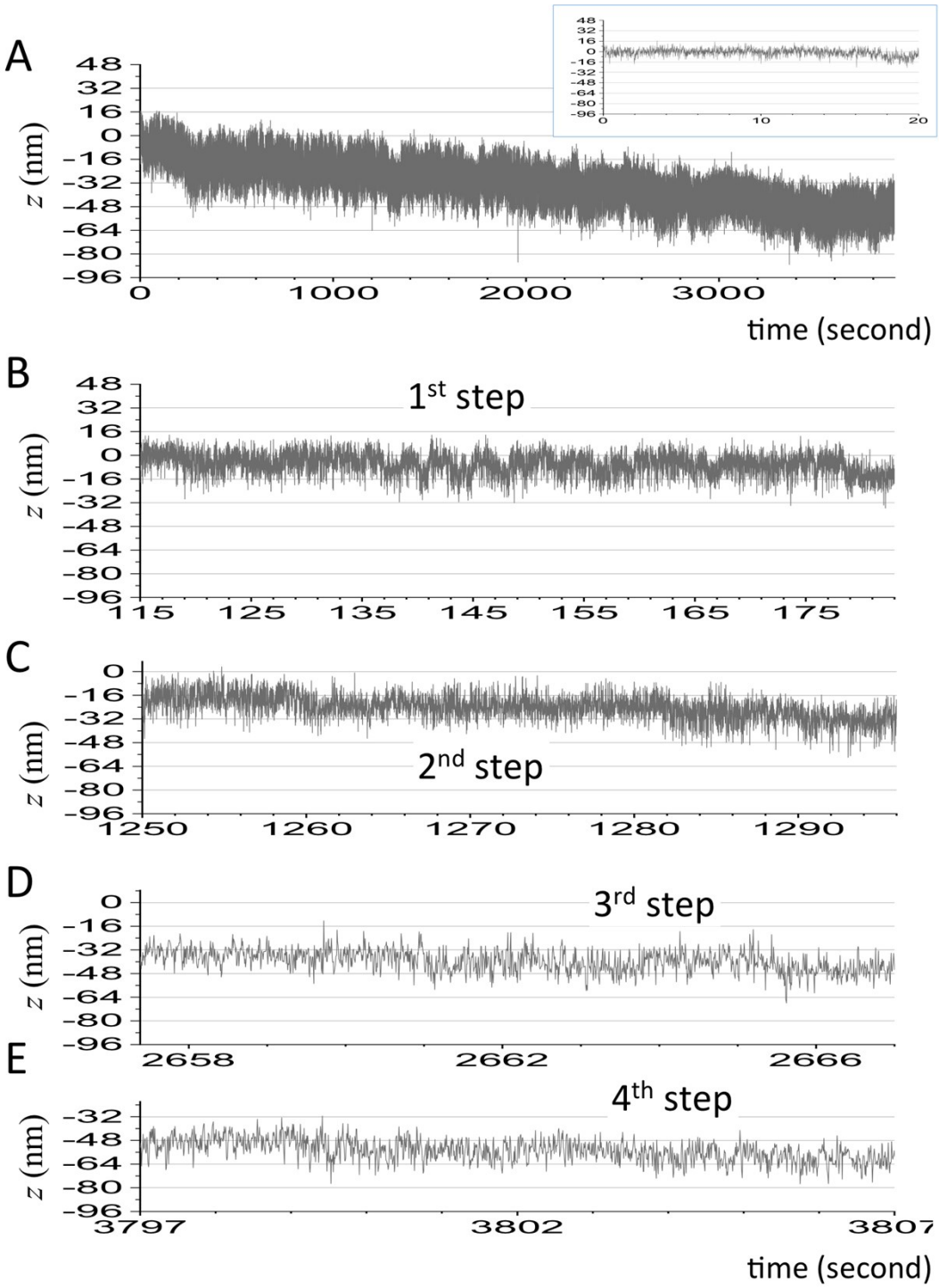


**Figure S5. Typical trajectory of the motor under an opposing force of 1.5 pN and a fuel concentration of 1 μM.** The top panel shows the whole trajectory (starting segment amplified in inset). Other panels show details of the motor's individual stepping events. A similar analysis of stable-dwell segments throughout this ~ 1 hour long trajectory finds good match to ~ 16nm intervals and two intermediate positions as shown in Figure 4 B – E.

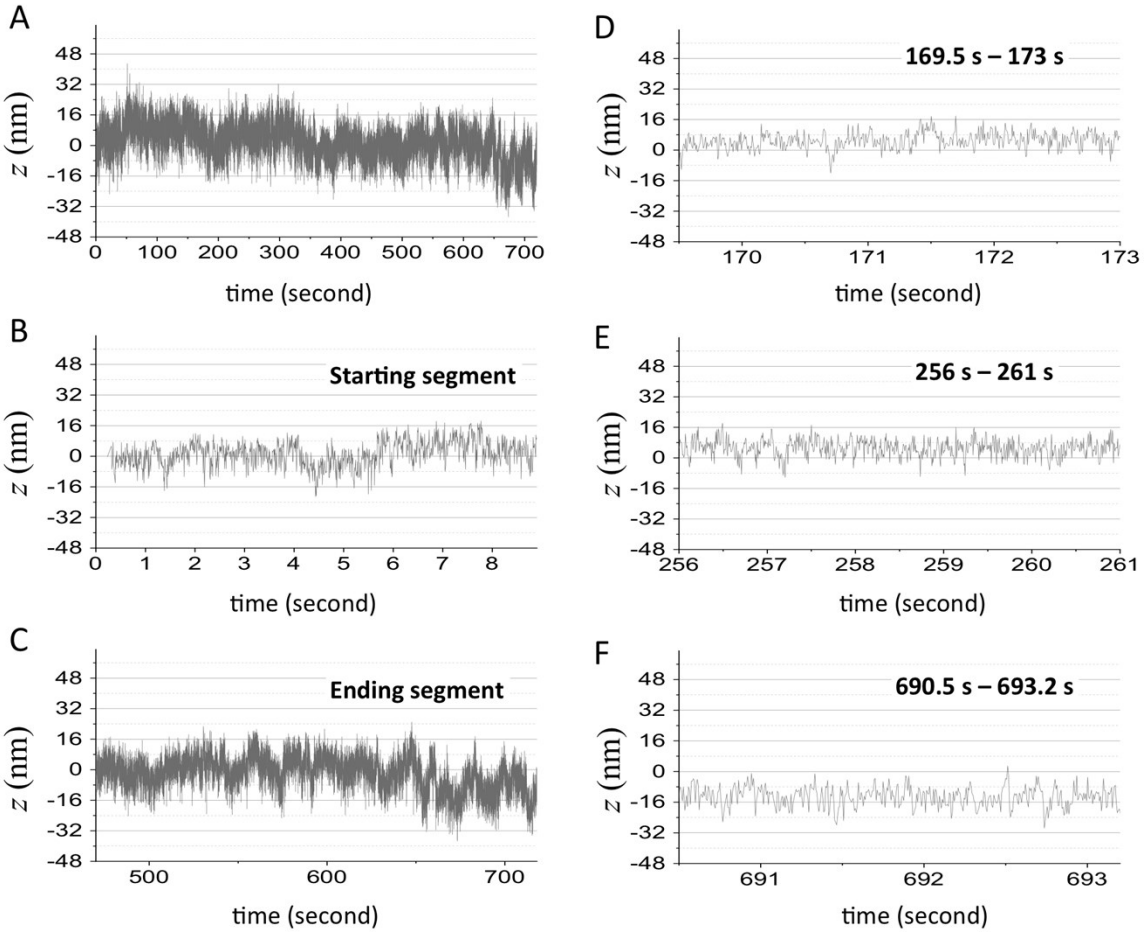


**Figure S6. A typical trajectory recorded under a nearly stalling force of 2 pN at 0.5 μM fuel.** Panel A shows the whole trajectory that is ~ 700 seconds long but barely makes a single forward step near the end. Panels B and C show details of the starting and ending segments. The whole trajectory is examined exhaustively to identify segments with stable dwell at intermediate positions other than 16nm intervals. Only three such segments are found with duration longer than 2.5 seconds. These segments, shown in panels D, E, F, have average displacements of ~ -12 nm and + 4 nm from the motor's starting position (i.e., the two-legged state as shown in Figure 1A), and fluctuate over a range of ~ 8 – 9 nm. The segment F is the same type of segments shown in Figure 4D; segments D, E correspond to force-assisted leg dissociation under fuel supply, which is similar to the force-induced dissociation identified in Figure S3 (again with average displacements equivalent of -12 nm in Figure 4D).

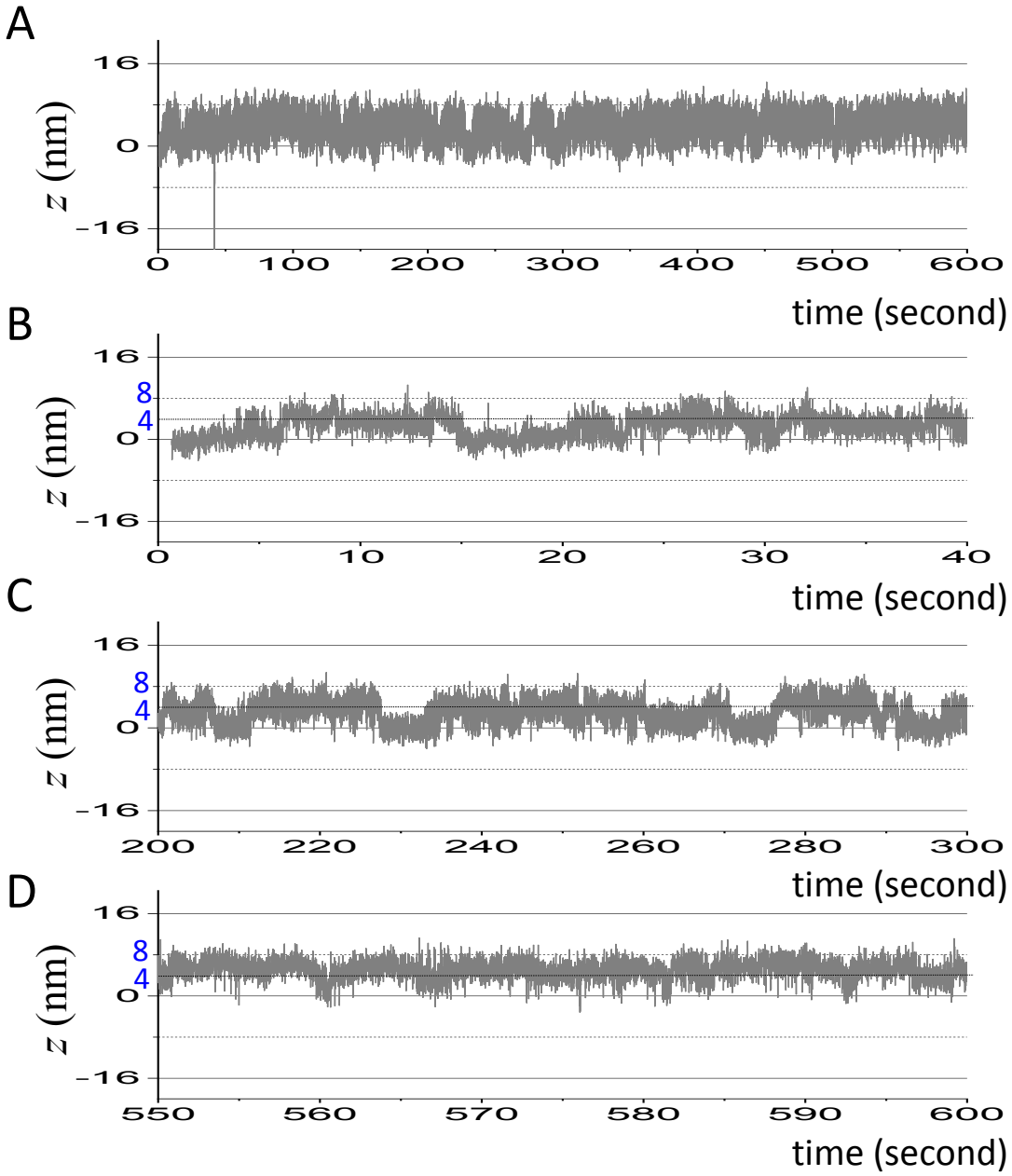
A
16
0
−16
z (nm)
0
100
200
300
400
500
600
time (second)
B
16
8
4
0
−16
z (nm)
0
10
20
30
40
time (second)
C
16
8
4
0
−16
z (nm)
200
220
240
260
280
300
time (second)
D
16
8
4
0
−16
z (nm)
550
560
570
580
590
600
time (second)

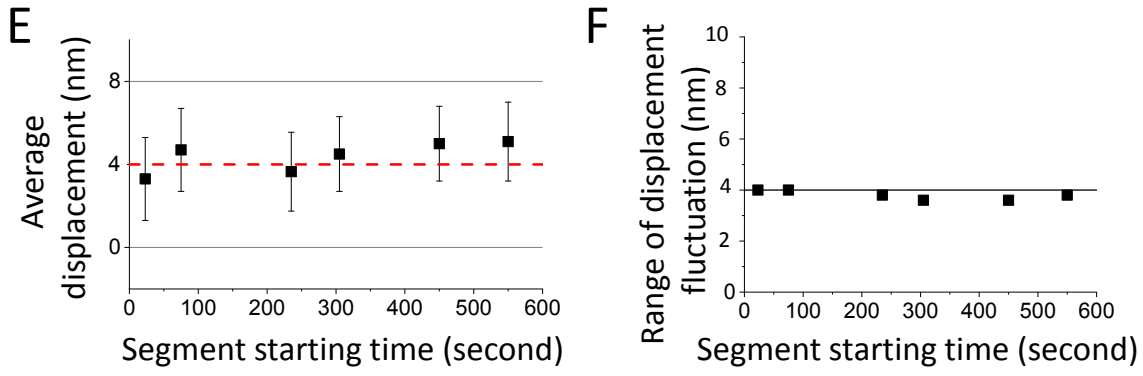
E
Average displacement (nm)
8
4
0
0
100
200
300
400
500
600
Segment starting time (second)
F
Range of displacement fluctuation (nm)
10
8
6
4
2
0
0
100
200
300
400
500
600
Segment starting time (second)

**Figure S7. A typical trajectory at an above-stall force of 3 pN and 0.5 μM fuel.**
The whole trajectory is presented in panel A, with details shown for representative segments at the start (panel B), in the middle (panel C), and near the end (panel D). The ~ 600s trajectory is stalled near the starting position (i.e., zero position at time zero), with amplified details showing frequent force-induced backward substeps and reverse forward substeps. Panel E gives average displacement (relative to the motor's starting position) of stable-dwell segments identified throughout the trajectory (segments yielding data from left to right: 24s – 38s, part of segment in panel B; 75s – 105s; 235s – 260s, part of segment in panel C; 305s – 330s; 450s – 470s; 550s – 600s, i.e., segment in panel D). Panel F gives the range of displacement fluctuations of these segments, namely two times the root-mean-square-displacement (RMSD) of each segment from its average position. The average displacement around + 4 nm (panel E) suggests a force-assisted leg dissociation as found in Figure S6 (similar to the force-induced dissociation identified in Figure S3, with + 4nm displacement equivalent of -12 nm in Figure 4D). Like segments in Figure S3, the starting segment (panel B) shows ~ 4nm backward substeps while the middle and ending segments (panels C, D) show similar backward steps with slightly larger displacement. This trend, which is probably due to elongated effects of the force, is also indicated by the average displacement in panel E. The range of displacement fluctuation at this above-stall force is ~ 4 nm (panel F), which is about half the value for 2 pN in Figure S6 and also smaller than the values for 1.5 pN with or without fuel (Figure 4E, Figure S3). Under the above-stall force of 3 pN, the trajectory shows no full backward step of 16nm because there is no track behind the motor's rear leg at the 1$^{st}$ binding site (see Figure 1A).

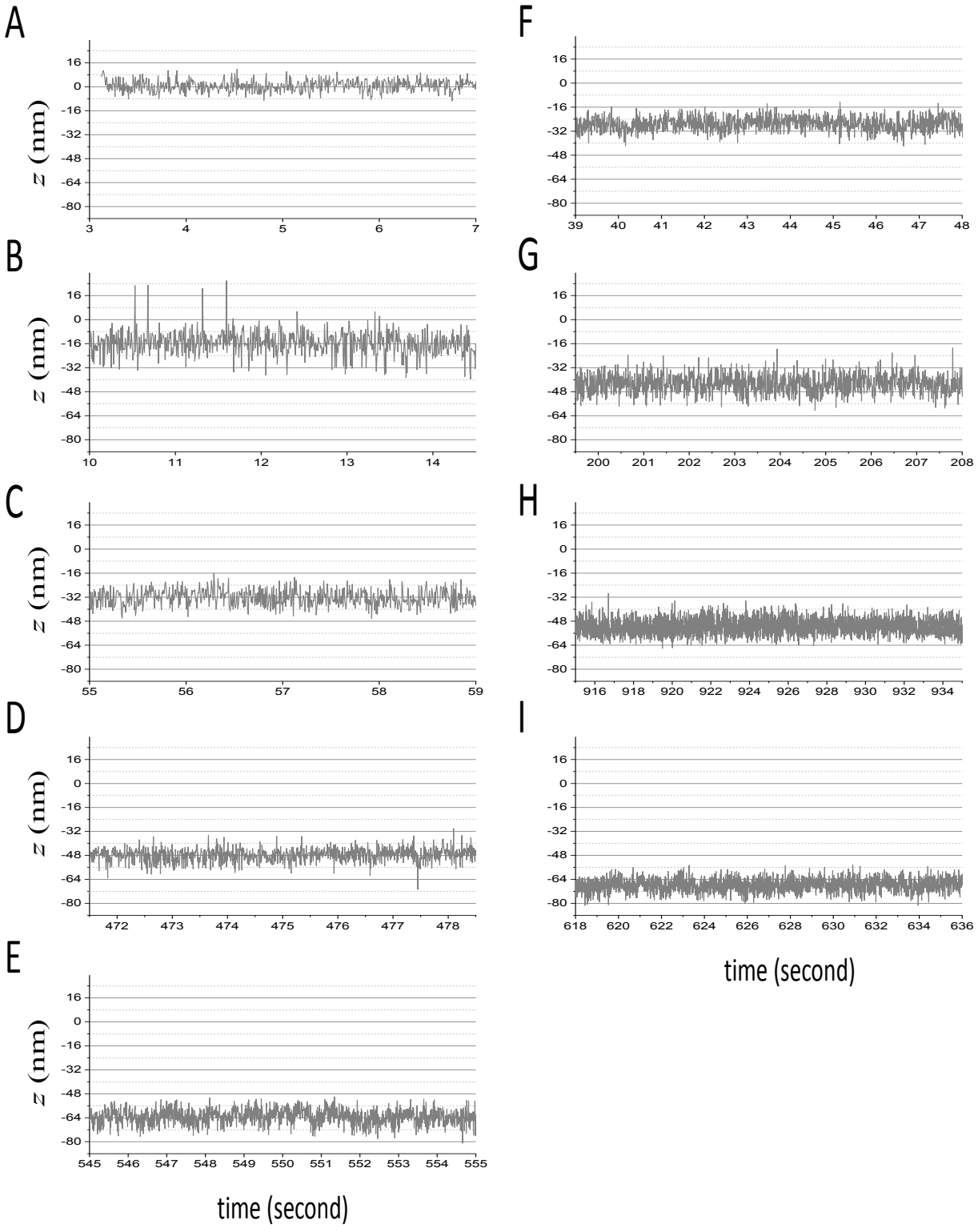


**Figure S8. Stable-dwell segments identified from the trajectory in Figure 2A.** An exhaustive examination of the 600s-long trajectory identifies a total of 17 segments that dwell stably at a reasonably fixed position over a duration longer than 4 seconds. For the 17 segments, 5 are found

at 16nm intervals, and 12 are found at intermediate positions (but only for four different positions). Panels A–E show all the 5 segments that dwell at 16nm intervals and last longer than 4 seconds. Panels F–I show four representative segments that dwell at intermediate positions. The segments in panels A–E yield the position data in Figure 4B. The segments in panels F–I yields four sets of displacement/fluctuation data in Figure 4C, D, E (segment F for solid rightward triangles in Figure 4D, E; segment G for empty spheres in Figure 4D, E; segment H for solid leftward triangles in Figure 4C, E; segment I for empty leftward triangles in Figure 4C). The other eight segments for intermediate positions (not shown here) yield other data in Figure 4C, D, E (Figure 4C: segment between 497.1s-504s for empty downward triangles, segment between 516s-533s for empty upward triangles, segment between 855s-862s for solid stars, segment between 982s-988s for solid diamond; Figure 4D, F: segment between 231s-242s for empty triangles, segment between 339.7s-344.2s for solid spheres, segment between 384s-390 s for empty stars, segment between 692s-700s for empty diamonds).

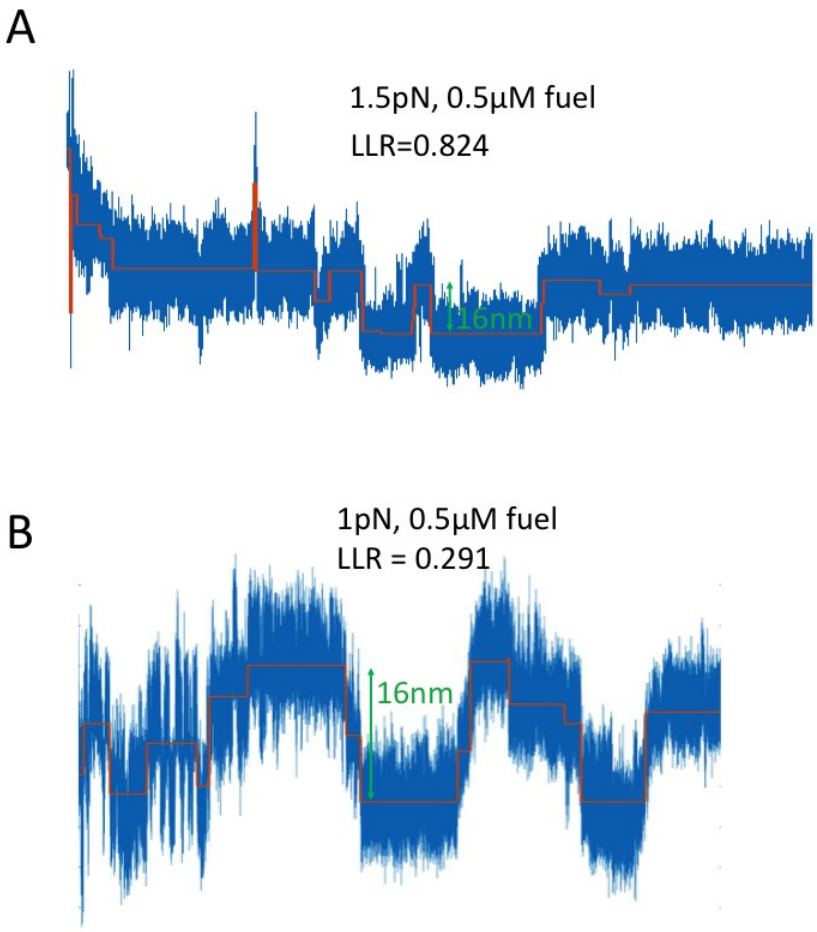


**Figure S9. Stepping analysis by a step finder algorithm[3].** Two representative trajectories are shown with stepping events identified by the algorithm (red lines; panel A is the same trajectory shown in Figure 2). The log-likelihood ratio (LLR) is shown for the stepping fitting (LLR > 0.08 is the criterion for stepping events). The trajectory in panel A has a sudden jump with displacement above the 16 nm step size, which is likely due to a recoverable bead fluctuation in the experiments.

A

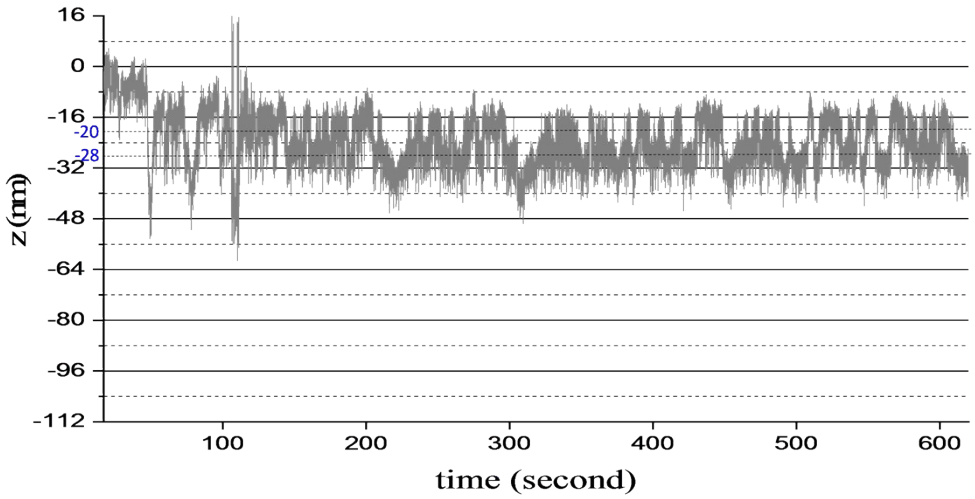
16
0
-16
-20
-28
-32
-48
-64
-80
-96
-112
z (nm)
100
200
300
400
500
600
time (second)

B

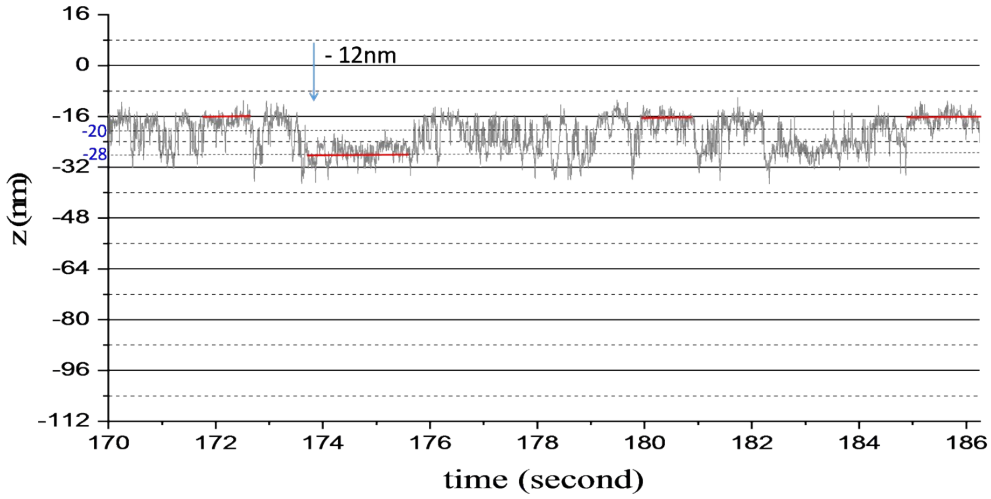
16
0
- 12nm
-16
-20
-28
-32
-48
-64
-80
-96
-112
z (nm)
170
172
174
176
178
180
182
184
186
time (second)

C

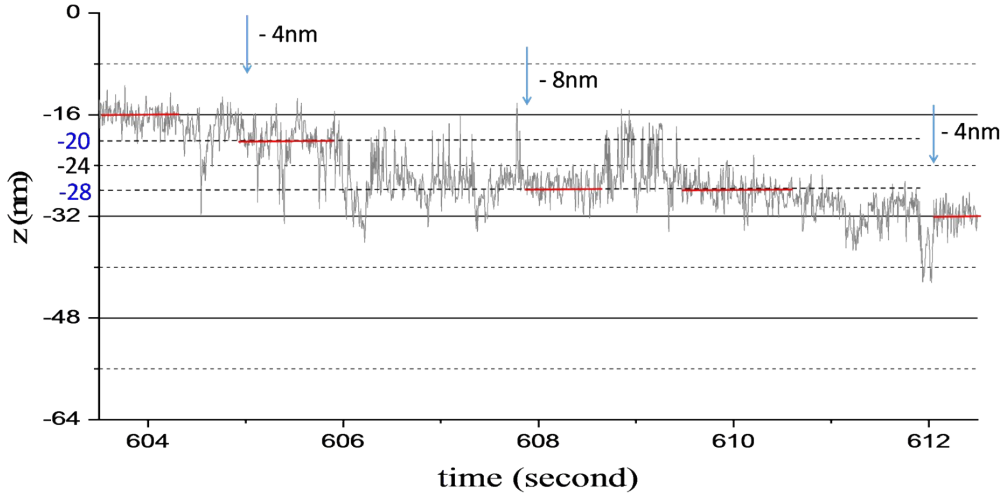
0
- 4nm
- 8nm
-16
-20
-24
-28
-32
- 4nm
-48
-64
z (nm)
604
606
608
610
612
time (second)

**Figure S10. A typical trajectory recorded under a nearly stalling force of 2 pN at 1 μM fuel.** Panel A shows the whole trajectory. Panels B and C show two segments in detail. Panel B is a failed step with the initial -16nm position fully recovered after a 12nm forward substep. Panel C is a successful 16nm forward step with three substeps. The red lines mark the motor's relatively stable dwelling positions. The vertical arrows indicate displacement between these dwelling positions.

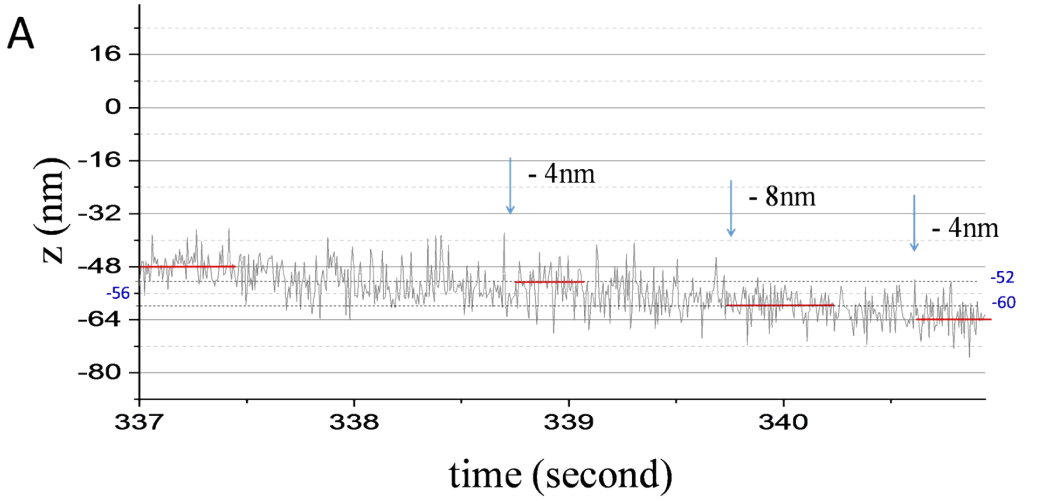
A
16
0
-16
-32
-48
-56
-64
-80
z (nm)
- 4nm
- 8nm
- 4nm
-52
-60
337
338
339
340
time (second)

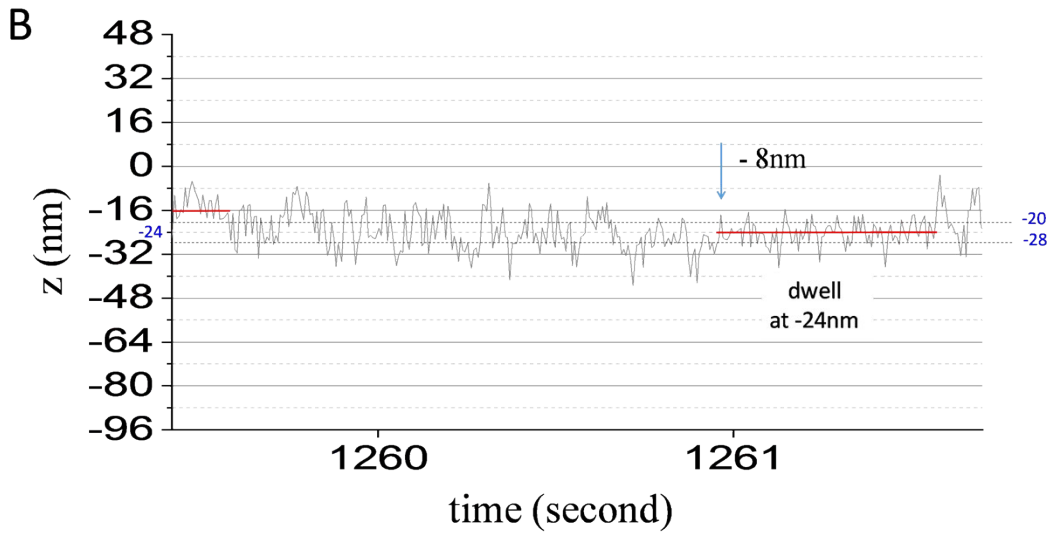
B
48
32
16
0
-16
-24
-32
-48
-64
-80
-96
z (nm)
- 8nm
-20
-28
dwell
at -24nm
1260
1261
time (second)

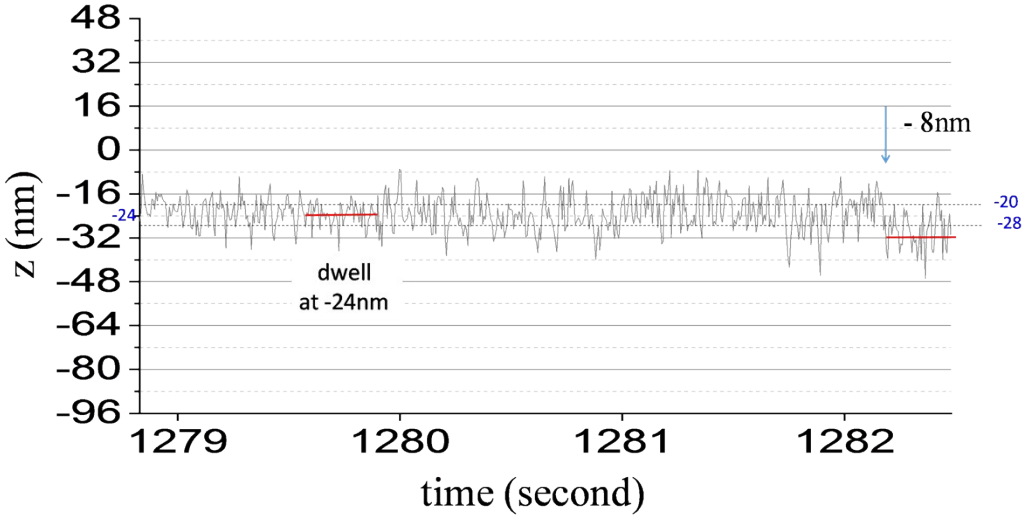
48
32
16
0
-16
-24
-32
-48
-64
-80
-96
z (nm)
- 8nm
-20
-28
dwell
at -24nm
1279
1280
1281
1282
time (second)

**Figure S11. Detailed stepping segments from the trajectory in Fig. 2A (panel A, for 1.5 pN and 0.5 μM fuel) and from the trajectory in Figure S5B (panel B, for 1.5 pN and 1 μM fuel).** Panel A shows a 16nm forward step with three substeps. Panel B is a 16nm forward step by two 8nm half steps (upper and lower plots for the same segment continuing in time). The red lines mark the motor's relatively stable dwelling positions. The vertical arrows indicate displacement between these dwelling positions.

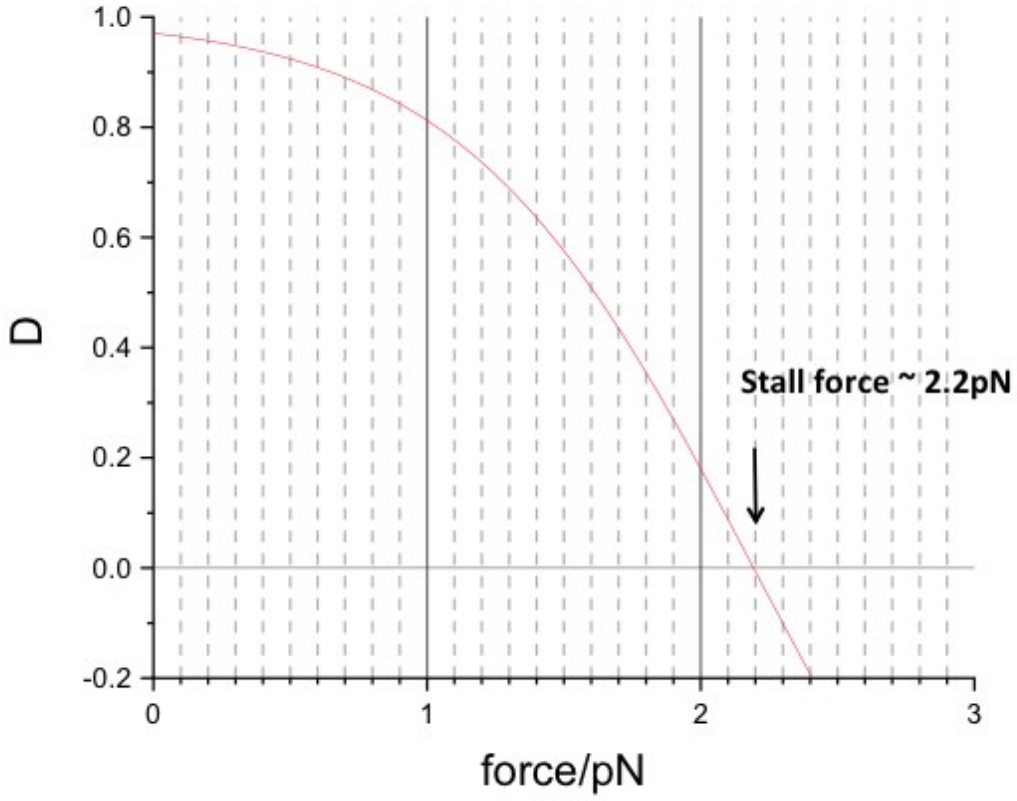


**Figure S12. The motor's load-dependent directionality and stall force estimated from biases associated with two equal-sized ~ 8nm half steps.** The two biases are reduced by the opposing force $f$ *as* $\alpha(f) = \alpha_0 \exp(-f\delta_1/k_BT)$ and $\beta(f) = \beta_0 \exp(-f\delta_2/k_BT)$. Here $\delta_1 = \delta_2 = 8$ nm are the displacement for two equal-sized half steps, $\alpha_0 \sim 100$ and $\beta_0 \sim 50$ are the zero-load biases from a previous ensemble fluorescence study[4], $T = 25$ °C is temperature for the present study, and $k_B$ is Boltzmann constant. The motor's directionality[5], defined as the net probability for a forward full step, is $D = (\alpha\beta - 1)/[(\alpha + 1)(\beta + 1)]$. The red curve shows the directionality as a function of opposing force predicted using the force-dependent biases. The directionality drops with the opposing force rises, and reaches zero at the stall force (~ 2.2 pN).

**References**


1. Charlie Gosse and Vincent Croquette, *Biophysical Journal*, 2002, **82**, 3314–3329.
2. Xiaodan Zhao, Xiangjun Zeng, Chen Lu and J. Yan, *Nanotechnology*, 2017, **28**, 414002.
3. TANUJ AGGARWAL, DONATELLO MATERASSI, ROBERT DAVISON, THOMAS HAYS and M. SALAPAKA, *Cellular and Molecular Bioengineering*, 2012, **5**, 14-31.
4. M. H. Liu, J. Cheng, S. R. Tee, S. Sreelatha, I. Y. Loh and Z. S. Wang, *ACS Nano*, 2016, **10**, 5882-5890.
5. Zhisong Wang, Ruizheng Hou and Iong Ying Loh, *Nanoscale*, 2019, **11**, 9240-9263.